Thin Solid Films 579 (2015) 136–143

Contents lists available at ScienceDirect

Thin Solid Films

journal homepage: www.elsevier.com/locate/tsf

A comparative study of $CF_4/O_2/Ar$ and $C_4F_8/O_2/Ar$ plasmas for dry etching applications

Inwoo Chun [a], Alexander Efremov [b], Geun Young Yeom [c], Kwang-Ho Kwon [a,*]

[a] Department of Control and Instrumentation Engineering, Korea University, 2511 Sejong-Ro, Sejong 339-700, South Korea
[b] Department of Electronic Devices & Materials Technology, State University of Chemistry & Technology, 7F. Engels St., 153000 Ivanovo, Russia
[c] Department of Advanced Materials Science & Engineering, Sungkyunkwan University, Suwon 440-746, South Korea

ARTICLE INFO

Article history:
Received 20 February 2014
Received in revised form 23 February 2015
Accepted 23 February 2015
Available online 1 March 2015

Keywords:
Tetrafluoromethane
Perfluorocyclobutane
Plasma diagnostics
Modeling
Reaction kinetics
Plasma modeling

ABSTRACT

The effect of the O_2/Ar mixing ratio in $CF_4/O_2/Ar$ and $C_4F_8/O_2/Ar$ inductively coupled plasmas with a 50% fluorocarbon gas content on plasma parameters and active species densities, which influence dry etching mechanisms, was analyzed. The investigation combined plasma diagnostics using Langmuir probes and zero-dimensional plasma modeling. It was found that, in both gas systems, the substitution of Ar for O_2 results in a similar change in the ion energy flux but causes the opposite behavior for the F atom flux. The mechanisms of these phenomena are discussed with regards to plasma chemistry.

1. Introduction

Fluorocarbon (FC) gases such as CF_4 and C_4F_8 are widely used in the microelectronic industry for the dry patterning of dielectric (SiO_2, Si_3N_4) thin films [1,2]. In most of the processes described in Refs. [2–4], these gases are combined with O_2 with the aim of increasing the F atoms' yield and suppressing polymerization on the surfaces which are in contact with the plasma. Recently, in order to satisfy the increasingly demanding requirements concerning device dimensions and performance, many dry etching processes require optimization through the appropriate choice of working gas and input process conditions. In this framework, an understanding of the plasma chemistry mechanisms involved in various gas systems is important for future progress.

From existing experimental and modeling studies (for example, from Refs. [5–14]), the basic properties of CF_4- and C_4F_8-containing plasmas can be briefly summarized as follows:

1) Under the conditions of a low-pressure ($p < 50$ mTorr or 6.7 Pa) gas discharge plasma, the C_4F_8 is more polymerizing than CF_4 because of its lower F/C ratio [15]. From Refs. [16–18], one can initially assume that the greater polymerizing effect of C_4F_8 is connected with the higher CF and CF_2 radical densities. However, since the above-mentioned studies employed different process conditions, this argument needs additional justification. It was also found that the dilution of C_4F_8 by approximately 40–50% Ar shifts the dominant surface process pathway from polymerization to etching [4,19].
2) The densities of F atoms in pure CF_4 and C_4F_8 plasmas are almost equal [20]. At low input powers ($W < 500$ W), a slightly higher F atom density has been measured in the CF_4 plasma, while at high power ($W > 1000$ W) the opposite occurs. A growth in gas pressure increases the F atom density in the CF_4 plasma [16,20], but suppresses it in the C_4F_8 plasma [21]. The reasons for this difference, along with the peculiarities of F atom kinetics in both gas systems, has not yet been studied.
3) The addition of O_2 to the CF_4-based gas mixture results in the non-monotonic behavior of the F atom density, which exhibits a maximum at 20–40% O_2 [5–9]. Most authors attribute this effect to the stepwise dissociation of the CF_x species due to their interaction with oxygen atoms [6,9]. However, the addition of O_2 to the C_4F_8-based gas mixture does not result in a similar effect [22]. This phenomenon has not been analyzed in terms of plasma chemistry and it therefore remains unclear.

We would also like to note that the effect of O_2 on the plasma parameters and composition of these substances has been well-examined only for binary (FC/O_2) or ternary ($FC/O_2/Ar$) gas mixtures, where an increase in the O_2 mixing ratio is accompanied by a proportionally decreasing FC gas component. At the same time, the ternary gas systems provide more pathways for changes in the gas-mixing ratios, in order

* Corresponding author.
E-mail address: kwonkh@korea.ac.kr (K.-H. Kwon).

http://dx.doi.org/10.1016/j.tsf.2015.02.060
0040-6090/

to obtain optimal process conditions. For example, one can keep the fraction of FC gas constant, but change the ratio between O_2 and Ar. It is clear that, since the composition of the feed gas is different compared with the simple FC/O_2 mixture, some principal differences in plasma parameters (through the electron energy distribution function and mean electron energy) and densities of plasma active species can take place. This is why the relationships between the plasma parameters and the composition of the three-component FC/O_2/Ar gas mixture with an FC gas component of constant magnitude require additional investigation.

The goal of this work is the comparative study of $CF_4/O_2/Ar$ and $C_4F_8/O_2/Ar$ inductively coupled plasmas, with an aim of understanding the influence of the substitution of Ar for O_2 at a fixed 50% fraction of the fluorocarbon gas on the plasma parameters and densities of active species, in a reactor of given geometry and under identical operating conditions. The focus is on the parameters directly influencing dry etching mechanisms, such as the ion energy flux, F atom density, and the CF_x ($x = 1$–3) radical density. We also attempt a model-based analysis of the formation-decay kinetics for neutral species in order to explain the differences in plasma composition.

2. Experimental details and modeling

2.1. Experimental setup and procedures

The experiments were performed in a planar inductively coupled plasma (ICP) reactor used in previous work [23,24]. The reactor had a cylindrical chamber ($r = 15$ cm), made from anodized aluminum. A 5-turn-copper coil was located on the top of the chamber, above the 10-mm-thick horizontal quartz window. The coil was connected to a 13.56 MHz power supply in order to sustain the plasma. The distance, l, between the window and the bottom electrode, which was used as a substrate holder, was 12.8 cm. The bottom electrode was connected to another 12.56 MHz power supply in order to control the negative dc bias on the etched wafer.

The experiments were performed at a fixed total gas flow rate ($q = 40$ sccm), gas pressure ($p = 6$ mTorr or 0.8 Pa), and input power ($W = 900$ W). The input power density $W' = W/\pi r^2 l$ then became 0.9 W/cm^3. In order to imitate actual etching conditions, the bottom electrode was biased by $W_{dc} = 200$ W. The $CF_4/O_2/Ar$ or $C_4F_8/O_2/Ar$ gas compositions were set by adjusting the partial flow rates. The CF_4 or C_4F_8 flow rates were fixed at 20 sccm while the flow rates of the O_2 and Ar were variably set to a combined total of $q_{O_2} + q_{Ar} =$ 20 sccm. Therefore the proportion of CF_4 ($y_{CF_4} = q_{CF_4}/q$) or C_4F_8 ($y_{C_4F_8} = q_{C_4F_8}/q$) in the feed gas was always 0.5, and the remaining half of each gas mixture was composed of various amounts of Ar and O_2

The plasma parameters were determined by a double Langmuir probe (LP) (DLP2000, Plasmart Inc.). The probe tip was installed through a hole in the sidewall of the chamber, 5.7 cm above the bottom electrode and centered in a radial direction. In order to ensure that the LP results were not affected by the formation of the FC polymer film on the tip surface, we conducted a set of preliminary experiments, where the current–voltage (I – V) curves were recorded continuously at fixed-feed gas composition and operating parameters. Even for the non-oxygenated plasmas, the differences between the results of such measurements did not exceed the standard experimental error for a period of at least 10 min after the plasma was turned on. Also, throughout the main experimental procedure, the probe tip was cleaned in 50% Ar + 50% O_2 plasma before and after each measurement. The output data were the electron temperature (T_e), ion current density (J_+), floating potential (U_f), and total positive ion density (n_+). The treatment of the I – V curves was based on Johnson & Malter's double probe theory [25], and the Allen–Boyd–Reynolds approximation for the ion saturation current density [26]. These assume $J_+ \approx 0.61 e n_+ \upsilon$, where υ is the ion Bohm velocity. In our previous studies [23,24], it was shown that such an approach can be reasonably applied even for more electronegative plasmas than those used in this study. The effective ion mass needed to determine υ was evaluated simply through the mole fractions of the corresponding neutral species.

The negative dc bias voltage was measured using the auto-matching RF control system (AMN-CTR, Youngsin ENG.). It was found that, in both gas systems, the I – V curves are not sensitive to W_{dc}. This result corresponds to the domination of the collisional power loss over the energy dissipated through the ion and electron fluxes to the reactor walls.

2.2. Plasma modeling

To obtain the densities of the active species, we developed a simplified zero-dimensional model operating with the volume-averaged plasma parameters. Similar to our previous papers [9,11,23,24], the model was based on the Maxwellian electron energy distribution function (EEDF), and used the experimental results of T_e and n_+ directly as input parameters. Although the experimental EEDFs are not exactly Maxwellian, such a simplification for both CF_4-based and C_4F_8-based low-pressure ($p < 50$ mTorr or 6.7 Pa) ICPs provides reasonable agreement between the diagnostic results and theoretical modeling [10–12, 16,27]. Also, based on published studies on plasma chemistry in CF_4 and C_4F_8 gases, as well as in mixtures with Ar and O_2 [5–14], we accepted the following assumptions:

1) For the given range of process conditions, the electronegativity of both gas systems is low enough to assume $n_- \ll n_e \approx n_+$. Our previous work [11] gave $n_-/n_e \sim 0.1$ for a 50% CF_4 + 50% Ar gas mixture at $p = 15$ mTorr (~2.0 Pa) and $W' = 0.8$ W/cm^3. Kimura and Noto [5] reported $n_-/n_e \sim 0.13$ for 50% CF_4 + 50% O_2 plasma at $p = 8$ mTorr (~1.0 Pa) and $W' = 0.8$ W/cm^3. Furthermore, Rauf and Ventzek [14] found $n_-/n_e \sim 0.03$ for 50% C_4F_8 + 50% Ar ICP at $p = 10$ mTorr (~1.3 Pa) and $W' = 0.6$ W/cm^3. Since all these values relate to higher pressures and lower power densities than those used in the present study, we can assume $n_-/n_e < 0.1$ with confidence.
2) The half-diluted CF_4 and C_4F_8 gases do not form a continuous fluorocarbon film on the chamber walls under plasma conditions [4,19]. This allows one to describe the heterogeneous chemistry of atoms (F, C, O) and radicals (CF_3, CF_2, CF) in terms of the conventional first-order recombination with the same sticking probabilities (γ) for both gas systems. The latter were obtained from Refs [5,11]. Since the sticking probability for C_2F_3 radicals is not known, the heterogeneous loss of these species was not included in the models. The calculations showed that accounting for $\gamma_{C_2F_3} = 0.05$ (as for CF_3), with the addition of $C_2F_3 \rightarrow C_2F_3(s)$ and $C_2F_3(s) + F \rightarrow C_2F_4$ in the reaction list (Table 1), does not influence principally the model-predicted densities of the main plasma active species for both gas systems.
3) The temperature of the neutral ground-state species (gas temperature, T) is independent of the feed gas composition [9,11]. Since experimental data on gas temperature were not available during this study, we took $T = 700$ K as the typical value for close ranges of p and W' in ICP etching reactors with similar geometry [5,9,11].

The steady-state densities of neutral species ($dn/dt = 0$) were obtained from the system of chemical kinetics equations in the general form of $R_F - R_D = (k_s + 1/\tau_R)n$, where R_F and R_D are the volume-averaged formation and decay rates in bulk plasma for a given type of species, n is their density, k_S is the first-order heterogeneous decay rate coefficient, and $\tau_R = \pi r^2 lp/q$ is the residence time. The list of processes included in the model is given in Table 1. The rate coefficients for electron impact reactions (R1–R23), were calculated as functions of T_e using fitting expressions in the form of $k = AT_e^B \exp(-C/T_e)$ [5, 17,27]. The rate coefficients for R24–R63 were taken from the NIST chemical kinetics database [28]. The rate coefficients for the heterogeneous loss of atoms and radicals R64–R70 were calculated as $k_S = [(\Lambda^2/D) + (2r/\gamma\upsilon_T)]^{-1}$, where D is the effective diffusion coefficient

Table 1
Reduced reaction set for the modeling of neutral species chemistry in $CF_4/Ar/O_2$ and $C_4F_8/Ar/O_2$ plasmas.

Process		Rate coefficient [cm^3/s]			
		ε_{th} [eV]	A	B	C
Electron-impact reactions					
R1	$C_4F_8 + e = 2C_2F_4 + e$	2.16	8.71×10^{-8}	0.042	8.572
R2	$C_4F_8 + e = C_3F_6 + CF_2 + e$	3.25	8.71×10^{-8}	0.042	8.572
R3	$C_3F_6 + e = C_2F_4 + CF_2 + e$	4.53	1.07×10^{-8}	0.23	7.451
R4	$C_2F_4 + e = 2CF_2 + e$	3.06	1.32×10^{-8}	0.412	6.329
R5	$C_2F_4 + e = C_2F_3^+ + F + 2e$	15.57	3.03×10^{-9}	0.874	16.41
R6	$C_2F_3 + e = CF_2 + CF + e$	3.06	3.30×10^{-8}	0.412	6.329
R7	$CF_4 + e = CF_3 + F + e$	5.60	1.38×10^{-8}	0	16
R8	$CF_4 + e = CF_2 + 2F + e$	9.50	2.22×10^{-10}	0.99	14.77
R9	$CF_4 + e = CF_3^+ + F + 2e$	15.9	9.36×10^{-8}	0	20.4
R10	$CF_4 + e = CF_3 + F^+ + 2e$	23.10	9.79×10^{-10}	0.94	34.67
R11	$CF_3 + e = CF_2 + F + e$	3.80	6.48×10^{-8}	−0.959	11.25
R12	$CF_2 + e = CF + F + e$	5.40	8.11×10^{-9}	0.386	8.739
R13	$CF_2 + e = C + 2F + e$	11.00	1.39×10^{-8}	−1.164	49.87
R14	$CF + e = C + F + e$	5.60	1.63×10^{-8}	−0.002	13.05
R15	$F_2 + e = 2F + e$	4.34	1.08×10^{-8}	−0.296	4.464
R16	$O_2 + e = 2O + e$	6.40	1.52×10^{-9}	0	4.15
R17	$O_2 + e = O + O(1d) + e$	8.57	2.04×10^{-8}	0	8.18
R18	$CO_2 + e = CO + O + e$	13.50	1.87×10^{-8}	0	13.89
R19	$CO + e = C + O + e$	13.50	1.87×10^{-8}	0	13.89
R20	$O + e = O(1d) + e$	1.97	4.47×10^{-9}	0	2.29
R21	$FO + e = F + O + e$	4.30	6.16×10^{-9}	0	4.30
R22	$CFO + e = CO + F + e$	5.40	8.11×10^{-9}	0.386	8.739
R23	$CF_2O + e = CFO + F + e$	3.80	6.48×10^{-8}	−0.959	11.25
Bulk atom-molecular, radical-molecular, and radical-radical reactions					
R24	$C_2F_3 + F = C_2F_4$	1.00×10^{-12}			
R25	$C_2F_4 + O = CF_2O + CF_2$	2.51×10^{-12}			
R26	$C_2F_4 + O(1d) = CF_2O + CF_2$	2.51×10^{-11}			
R27	$C_2F_4 + F = CF_2 + CF_3$	3.98×10^{-11}			
R28	$C_2F_4 + C = C_2F_3 + CF$	1.00×10^{-10}			
R29	$F_2 + CF_3 = CF_4 + F$	6.31×10^{-14}			
R30	$F_2 + CF_2 = CF_3 + F$	7.94×10^{-14}			
R31	$F_2 + CF = CF_2 + F$	3.98×10^{-12}			
R32	$F_2 + O = FO + F$	1.00×10^{-16}			
R33	$F_2 + O(1d) = FO + F$	7.94×10^{-12}			
R34	$F_2 + CFO = CF_2O + F$	5.01×10^{-14}			
R35	$CF_3 + F = CF_4$	1.00×10^{-12}			
R36	$CF_3 + O = CF_2O + F$	3.16×10^{-11}			
R37	$CF_3 + O(1d) = CF_2O + F$	3.16×10^{-11}			
R38	$CF_2 + F = CF_3$	4.17×10^{-13}			
R39	$2CF_2 = C_2F_4$	5.01×10^{-14}			
R40	$CF_2 + CF = C_2F_3$	1.00×10^{-12}			
R41	$CF_2 + O = CFO + F$	3.16×10^{-11}			
R42	$CF_2 + O(1d) = CFO + F$	3.16×10^{-11}			
R43	$CF_2 + O = CO + 2F$	3.98×10^{-12}			
R44	$CF_2 + O(1d) = CO + 2F$	3.98×10^{-12}			
R45	$CF + F = CF_2$	5.01×10^{-15}			
R46	$CF + O = CO + F$	6.31×10^{-11}			
R47	$CF + O(1d) = CO + F$	2.00×10^{-11}			
R48	$CF + O_2 = CFO + O$	3.16×10^{-11}			
R49	$FO + O = F + O_2$	2.51×10^{-11}			
R50	$FO + O(1d) = F + O_2$	5.01×10^{-11}			
R51	$FO + FO = 2F + O_2$	2.51×10^{-12}			
R52	$2FO = F_2 + O_2$	2.51×10^{-16}			
R53	$CFO + CF_3 = CF_4 + CO$	1.00×10^{-11}			
R54	$CFO + CF_3 = CF_2O + CF_2$	1.00×10^{-11}			
R55	$CFO + CF_2 = CF_3 + CO$	3.16×10^{-13}			
R56	$CFO + CF_2 = CF_2O + CF$	3.16×10^{-13}			
R57	$CFO + O = CO_2 + F$	1.00×10^{-10}			
R58	$CFO + O(1d) = CO_2 + F$	1.00×10^{-10}			
R59	$2CFO = CF_2O + CO$	1.00×10^{-11}			
R60	$CFO + F = CF_2O$	7.94×10^{-11}			
R61	$CF_2O + O(1d) = F_2 + CO_2$	2.00×10^{-11}			
R62	$C + O_2 = CO + O$	1.58×10^{-11}			
R63	$CO + F = CFO$	1.29×10^{-11}			
Heterogeneous reactions					
R64	$F = F(s) + CF_3 = CF_4$ $+ CF_2 = CF_3$ $+ CF = CF_2$ $+ F = F_2$ $+ C = CF$ $+ C_2F_3 = C_2F_4$	$f(\gamma)$, $\gamma = 0.05$			

Table 1 (*continued*)

Process		Rate coefficient [cm^3/s]			
		ε_{th} [eV]	*A*	*B*	*C*
	+ O = FO				
R65	$CF_3 = CF_3(s) + F = CF_4$ + CF = C_2F_4 + C = C_2F_3	$f(\gamma)$, $\gamma = 0.05$			
R66	$CF_2 = CF_2(s) + F = CF_3$ + $CF_2 = C_2F_4$ + CF = C_2F_3 + O = CF_2O	$f(\gamma)$, $\gamma = 0.1$			
R67	CF = CF(s) + F = CF_2 + $CF_2 = C_2F_3$ + $CF_3 = C_2F_4$ + O = CFO	$f(\gamma)$, $\gamma = 0.1$			
R68	C = C(s) + F = CF + $CF_3 = C_2F_3$ + O = CO	$f(\gamma)$, $\gamma = 1$			
R69	O = O(s) + $O = O_2$ + F = FO + C = CO + CF = CFO + $CF_2 = CF_2O$	$f(\gamma)$, $\gamma = 0.1$			
R70	O(1d) = O	$f(\gamma)$, $\gamma = 1$			
R71	$CF_3^+ = CF_3$	υ/d_c, where			
R72	$F^+ = F$	$\upsilon \approx \sqrt{eT_e/m_i}$			
R73	$C_2F_3^+ = C_2F_3$	$d_c = 0.5rl/(rh_l + lh_r)$			

[29], $\Lambda^{-2} = (2.405/r)^2 + (\pi/l)^2$ is the diffusion length [29], and $\upsilon_T = (8k_BT/\pi m)^{1/2}$. All reaction pathways between the adsorbed (marked by the "s" index) and gaseous species inside R64–R69 were assumed to have equal probabilities of occurrence. The rate coefficients for the heterogeneous loss of ions R71–R73 were calculated as $k_S = \upsilon/d_c$, where $d_c = 0.5rl/(rh_l + lh_r)$. The correction factors for axial (h_l) and radial (h_r) sheath sizes are given by the low pressure diffusion theory [29].

The model quality was preliminarily tested using the experimental data on F atom density in CF_4/O_2 plasma [5], and both CF_2 and CF radical densities in C_4F_8/Ar plasma [14]. These studies were selected based on two main reasons. First, both studies were carried out in ICP reactors of similar geometry under a close range of experimental conditions. Secondly, the authors of both works also provided the measurements of T_e and n_e, which are required as input model parameters. As can be seen from Fig. 1, there is reasonable agreement between the measured and model-predicted species densities. Moreover, from Fig. 1(a) one can conclude that our model-predicted curve is closer to the experimental data of Ref. [5] than the results of their calculations. In our opinion, this is because they did not take into account the recombination of F and CF_x on the reactor walls, and assumed only the loss of these species in the fluorocarbon film growth process.

3. Results and discussion

Figs. 2 and 3 represent the results of plasma diagnostics using Langmuir probes. From Fig. 2, it can be seen that the substitution of Ar for O_2 results in decreasing T_e in the ranges of 3.6–3.4 eV for CF_4/O_2/Ar and 4.8–3.1 eV for C_4F_8/O_2/Ar plasma. The reason for this is an increase in the electron energy loss due to the low-threshold excitations (vibrational, electronic) for O_2 and other molecular species, which appear in a gas phase as products of plasma chemical reactions. It can also be seen that the total positive ion density (and thus, the electron density, since $n_+ \approx n_e$) decreases toward O_2-rich plasmas. Particularly, for the CF_4/O_2/Ar gas mixture, an increase in the O_2 content in the feed gas from 0–50% (i.e. the transition from the CF_4/Ar to the CF_4/O_2 system) results in $n_+ = 4.2 \times 10^{10}$–3.2×10^{10} cm^{-3}, which corresponds to $J_+ = 1.10$–0.95 mA/cm^2 (Fig. 3(a)). A similar change in the gas mixing ratios for C_4F_8/O_2/Ar plasma produces $n_+ = 4.2 \times 10^{10}$–3.7×10^{10} cm^{-3} and $J_+ = 1.21$–0.91 mA/cm^2. In our opinion, such effects are caused by a combination of at least two phenomena. First, the decreasing T_e suppresses ionization through decreasing the ionization rate coefficients for all types of neutral species. The high sensitivity of the ionization rate coefficients to T_e is because $\varepsilon_{iz} \approx$ 12–15 eV > $(3/2)T_e$, where ε_{iz} is the threshold energy for ionization [5,17], and $(3/2)T_e$ is the mean electron energy. Secondly, the substitution of Ar for O_2 probably results in an increase in the densities of electronegative species, caused by both the O_2 itself and oxygen-containing reaction products. This accelerates the decay rates of the positive ions and electrons through ion-ion recombination and dissociative attachment, respectively. Therefore, the changes in the gas-mixing ratios in CF_4/O_2/Ar and C_4F_8/O_2/Ar at a constant fluorocarbon component fraction result in similar effects on both T_e and n_e. In fact, this means that the features of the plasma compositions discussed below are mainly connected with the chemical properties of the original fluorocarbon molecules.

When comparing the gas systems for dry etching applications, an important issue is the efficiency of the ion bombardment which determines the contribution of the physical etching pathway to the overall process rate. In the ion-assisted chemical reaction, the role of ion bombardment may include the sputtering of the native surface atoms, the ion-stimulated desorption of low-volatility reaction products, and the destruction of the fluorocarbon film. From Refs. [30–32], it can be understood that the rate of the physical etching pathway is given by $Y_s\Gamma_+$, where $\Gamma_+ \approx J_+/e$ is the total flux of the positive ions on the etched surface and Y_s is the ion-type-averaged sputtering yield. For the ion bombardment energy, $\varepsilon_i < 500$ eV, one can assume Y_s to be proportional to the momentum transferred by the incident ion to the surface atom [31,33]. Therefore, the physical etching pathway can be characterized by the parameter $\sqrt{m_i\varepsilon_i}\Gamma_+$, where $\varepsilon_i \approx e|-U_f-U_{dc}|$. From Fig. 3(a), it can be seen that, in both gas systems, the parameter $-U_{dc}$ changes similarly but exhibits different absolute values (137–153 V and 145 –177 V for 0–50% O_2 in CF_4/O_2/Ar and C_4F_8/O_2/Ar plasmas, respectively). Such differences are directly reflected in the ion bombardment energies, which change in the ranges of 159–173 eV for the CF_4-based gas mixture and 175–196 eV for the C_4F_8-based substance. However, the weakly increasing ε_i does not compensate for the fall of Γ_+, and therefore the parameter $\sqrt{m_i\varepsilon_i}\Gamma_+$ decreases monotonically toward O_2-rich plasmas (Fig. 3(b)). Therefore, for both gas mixtures, the substitution of Ar for O_2 suppresses the physical

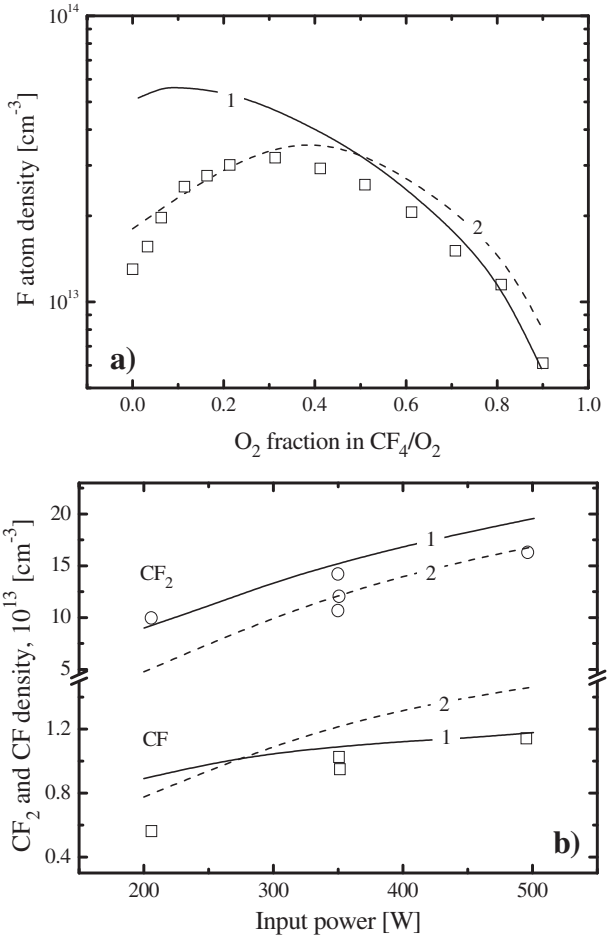

Fig. 1. The validation of plasma models with experimental data. Fig. a): The comparison of measured (dots)[5] and model-predicted (lines) fluorine atom densities in CF_4/O_2 inductively coupled plasma at $p = 5$ mTorr (~0.7 Pa), $W = 120$ W. 1: Model of Ref. [5], 2: Our model with T_e and n_e from Ref. [5] Fig. b): The comparison of measured (dots)[14] and model-predicted (lines) CF_2 and CF densities in 98% C_4F_8 + 2% Ar inductively coupled plasma at $p = 15$ mTorr (~2.0 Pa). 1: Model of Ref. [14], 2: Our model with T_e and n_e from Ref. [14].

etching pathway. Considering that the absolute values of Γ_+ in the low-oxygenated $C_4F_8/O_2/Ar$ plasmas are higher than those for $CF_4/O_2/Ar$, the first system demonstrates about 20% greater ion bombardment efficiency.

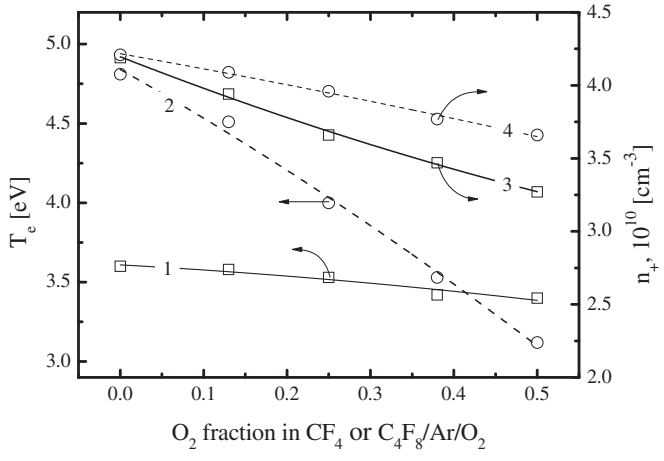

Fig. 2. Electron temperature (1, 2), and total positive ion density (3, 4), as functions of O_2 fraction in $CF_4/Ar/O_2$ (1, 3) and $C_4F_8/Ar/O_2$ (2, 4) gas mixtures at $p = 6$ mTorr (~0.8 Pa) and $W = 900$ W. In each gas mixture the fraction of fluorocarbon gas is fixed at 0.5. The lines are for visual guidance only.

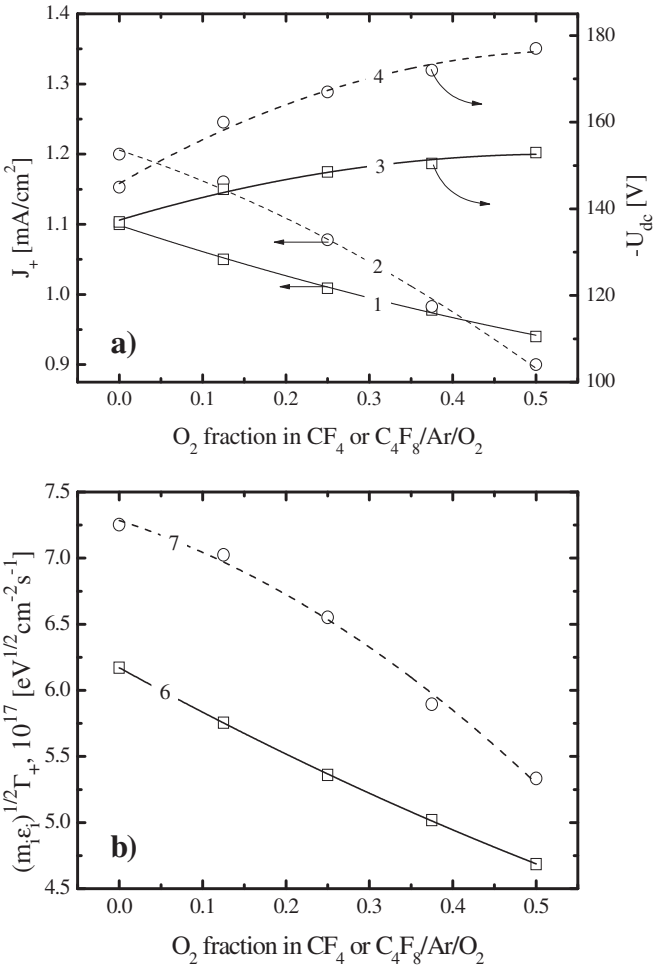

Fig. 3. Ion current density (1, 2), negative dc bias voltage (3, 4), and ion energy flux (5, 6), as functions of the O_2 component magnitude in $CF_4/Ar/O_2$ (1, 3, 5), and $C_4F_8/Ar/O_2$ (2, 4, 6), gas mixtures. The process conditions correspond to Fig. 2.

Fig. 4 represents the mole fractions of neutral species on the non-oxygenated (i.e. 50% CF_4 or C_4F_8 + 50% Ar) plasmas. The differences in the plasma compositions can be explained by accounting for the reaction scheme given in Table 1. The higher densities of C_2F_4 and C_2F_3 in the C_4F_8-based plasma are related with the direct formation of these species in the electron impact process R1–R3 and R5 with the participation of the original C_4F_8 molecules and their first-step dissociation products. The primary sources of CF_3 radicals in both systems are R7 and R10. The rates of R7 are similar while R10 is noticeably faster in the C_4F_8-based plasma. The reason for this is that the rate coefficient of the high-threshold R10 is very sensitive to differences in T_e in these systems. Apart from this, the CF_3 formation rate in the C_4F_8-based plasma is much more significantly affected by R27, R38, and R66 because of the much higher densities of C_2F_4 and CF_2, respectively. As a result, the difference between the magnitude of n_{CF_3} in the two systems is greater than five-fold. As for the differences in n_{CF_2} and n_{CF}, this situation is also sufficiently clear. Even assuming that CF_2 is mainly formed by electron impact in R4, R6, R8, and R11 from C_2F_4, C_2F_3, CF_4, and CF_3, the differences in the densities of the species discussed above must be reflected in the corresponding reaction rates and therefore in the densities of the reaction products. Moreover, the C_4F_8-based plasma provides both additional generation pathways for CF_2 (through R2 and R3) and higher rates of R27, R31, and R45. This is why the density of CF_2 in the C_4F_8-based plasma exceeds the corresponding value for the CF_4-based plasma by more than an order of magnitude. The gap between the CF densities reaches two orders of magnitude or greater. This is because

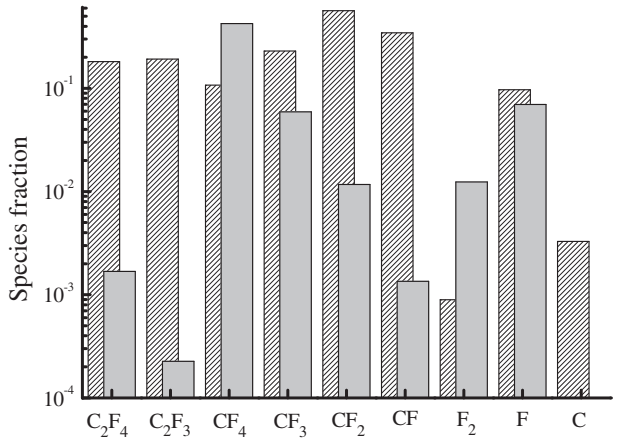

Fig. 4. Relative densities of neutral species in 50% CF_4 + 50% Ar (grey-filled bars) and 50% C_4F_8 + 50% Ar (patterned bars) plasmas at p = 6 mTorr (~0.8 Pa) and W = 900 W.

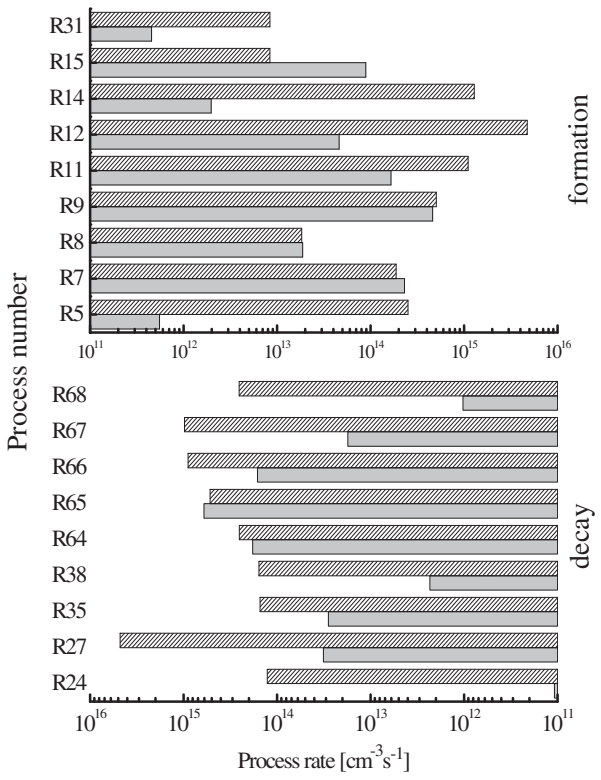

Fig. 5. Fluorine atoms kinetics in 50% CF_4 + 50% Ar (grey-filled bars) and 50% C_4F_8 + 50% Ar (patterned bars) plasmas at p = 6 mTorr (~0.8 Pa) and W = 900 W.

the difference between the rates of R6 and R12 due to the differences in $n_{C_2F_3}$ and n_{CF_2} densities, respectively. The number of F atoms in both gas systems is quite close, although some domination of this parameter in the C_4F_8-based plasma occurs. This fact is in good agreement with the experimental results reported in Ref. [20] for W > 800 W. Since the main formation pathway for F_2 molecules is F → F_2 recombination on the chamber walls (R64), the differences in n_{F_2} are due to the differences in their decay rates only. Accordingly, the lower F_2 density in the C_4F_8-based plasma results from the faster decay of these species due to interactions with CF_2 and CF in R30, R31, R38, and R45. And finally, the specific feature of the C_4F_8-based plasma is the high density of C atoms due to the electron impact dissociations of CF_2 (R13) and CF (R14). The combination of much higher values of n_{CF_2}, n_{CF}, and n_C makes the C_4F_8-based plasma a much stronger polymerizing system compared with CF_4-based plasma under the same operating conditions. This fact has been repeatedly confirmed by experiment [16,18].

Among the numerous neutral species formed in CF_4- and C_4F_8-based plasmas, F atoms are of primary interest for the analysis of the dry etching process. The knowledge of formation-decay mechanisms for F atoms allows one to understand and predict how the input process parameters, including the addition of O_2 in the feed gas, influence the etching rate through changes in the densities of chemically active species. Although the densities of F atoms in both systems were found to be quite similar, the kinetics of these species is principally different. From Fig. 5 it can be seen that, in the non-oxygenated 50% CF_4 + 50% Ar plasma, the main source of F atoms are the electron-impact dissociations of CF_4 (R7, R9) and CF_3 (R11). These processes constitute approximately 86% of the total F atom formation rate while the contribution from the CF_2 and CF radicals through R12–R14 does not exceed 5%. The remaining 9% comes from R15, which is supported by the high F → F_2 recombination rate in R64. The other R64 pathways are less effective due to the lower densities of the corresponding gaseous species. In the C_4F_8/Ar plasma, the dominant formation pathways for F atoms are R11, R12, and R14, with a total contribution of 88%. The reactions R7–R9 constitute approximately 9% and the R5 reaction adds only 3%. Therefore, a feature of the C_4F_8-based plasma is that the F atom formation rate is directly related to the densities of the unsaturated CF_x (x < 3) radicals. Since the latter are involved in numerous neutral-neutral reactions, the resulting F atom density is influenced by more reaction pathways than those in the CF_4-based plasma. F atom decay in the CF_4-based plasma is mainly caused by their heterogeneous recombination in R64–R66, while the rate of the fastest bulk process R35 is about 10 times less. This situation is a "classical" scheme for low-pressure plasmas in many gases [29]. In spite of this, the decay of F atoms in the C_4F_8-based plasma is controlled by the atom-molecular reaction R27, which provides about 60% of the total decay rate. The heterogeneous recombination in R64–R68 contributes 36%. Since the second reactant participating in R27, C_2F_4, is formed directly from C_4F_8 in R1, an increase in the density of C_4F_8 molecules accelerates the loss rate of the F atoms. This model-based conclusion is confirmed by the experimental data of Sasaki et al. [21]. In particular, they reported a decrease in n_F with increasing C_4F_8 gas pressure.

Fig. 6 illustrates the influence of O_2 content in the CF_4/Ar/O_2 gas mixture on the densities of neutral species. The substitution of Ar for O_2 at a constant fraction of CF_4 noticeably reduces the rates of R7, R9, and R11, even under the condition of low-oxygenated ($y_{O_2} < y_{Ar}$) plasmas (for example, a two-fold decrease at 12% O_2). This is due to the simultaneous decrease in n_e, n_{CF_4} (3.5×10^{13}–1.9×10^{13} cm^{-3} for 0–12% O_2), and n_{CF_3} (4.9×10^{12}–1.9×10^{12} cm^{-3} for 0–12% O_2). The density of CF_3 radicals decreases because of their decomposition in R36, R37, R53, and R54 with the participation of O, O(^{1}D), and CFO. The behavior of n_{CF_4} follows that of n_{CF_3} because the main sources of CF_4 molecules in the plasma chemical reactions are the CF_3 → CF_4 transformations in R64 and R66. At the same time, the addition of O_2 introduces new channels for the formation of F atoms involving CFO (R22) and CF_2O (R23), while also accelerating R15. The high formation rate for the CFO species is provided by R23 and R63, while CF_2O is effectively formed in R54, R59, and R60. The acceleration of R15 is due to the rapidly increasing F_2 density (n_{F_2} = 1.0×10^{12}–9.1×10^{12} cm^{-3} for 0–12% O_2), because of the formation of these species in R61 and R64. As a result, the total F atom formation rate increases compared with the CF_4/Ar plasma, which causes an increase in F atom density ($n_F = 5.8 \times 10^{12}$–2.6×10^{13} cm^{-3} for 0–12% O_2). The further addition of O_2 in the feed gas and the transition to the high-oxygenated plasmas ($y_{O_2} > y_{Ar}$) maintains all the previously mentioned tendencies for reaction rates while also introducing additional mechanisms for the formation of F atoms. Particularly, in the 50% CF_4 + 50% O_2 gas mixture (y_{O_2} = 0.5 and y_{Ar} = 0), the electron impact dissociation rate of the FO species (R21) reaches the R22 and R23 levels. The high formation rate and density of FO (8.1×10^{10}–6.4×10^{12} cm^{-3} for 12–50% O_2) are provided mainly by R33, R64, and R67. Simultaneously,

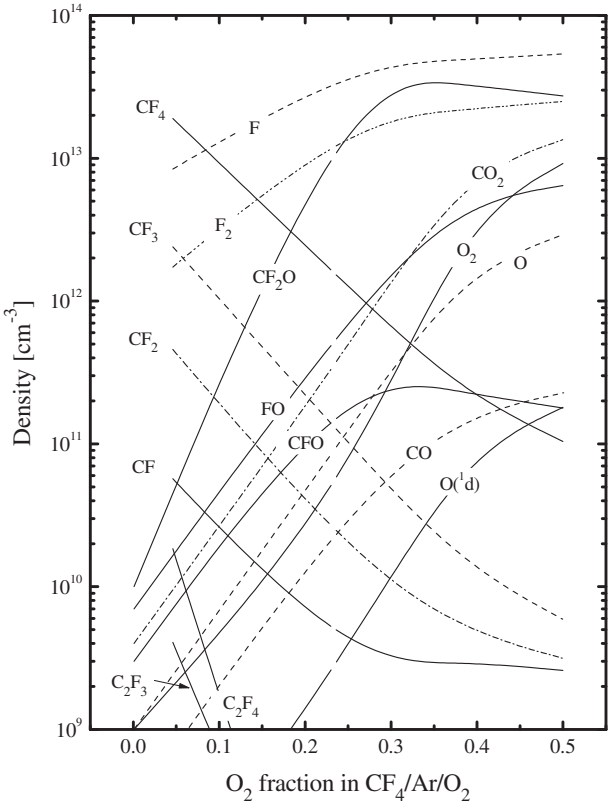

Fig. 6. Densities of neutral species as functions of O_2 component magnitude in $CF_4/Ar/O_2$. The process conditions correspond to Fig. 2.

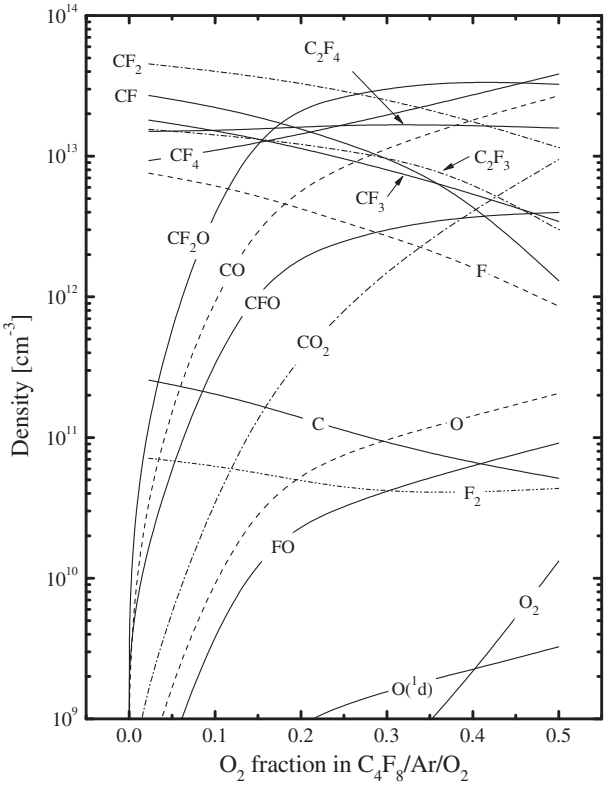

Fig. 7. Densities of neutral species as functions of O_2 component magnitude in $C_4F_8/Ar/O_2$. The process conditions correspond to Fig. 2.

the total effect of R21–R23 becomes greater than the sum of R7, R9, and R11. Apart from these, the rates of the atom-molecular processes R33, R49–R51, and R57 increase together with the increasing O_2 content in the feed gas and, finally, appear to be comparable with R21–R23. Therefore, the substitution of Ar for O_2 in the $CF_4/Ar/O_2$ gas mixture under the given conditions provides a continuous increase in the F atom formation rate and thus, the F atom density. Note that the opposite changes in F and CF_x densities create a favorable condition for etching, but not for polymerization.

Fig. 7 shows the changes in densities of neutral species in the $C_4F_8/Ar/O_2$ plasma with a variable O_2 component in the feed gas. The main peculiarity of this system is that the reactions R48 and R62 provide a more rapid loss of O_2 molecules than their electron-impact dissociation in R16 and R17. As a result the O_2 densities themselves, O and $O(^1D)$, appear to be much lower compared with those in the CF_4-based gas mixture, with the same proportion of O_2 in the feed gas. The lack of O and $O(^1D)$ makes the stepwise decomposition of CF_3 (R36, R37), CF_2 (R41–R44), and CF (R46, R47) slower than their electron-impact dissociations, even in the 50% C_4F_8 + 50% O_2 plasma. That is why the densities of CF_x radicals do not show a deep fall toward O_2-rich plasmas, as mentioned in Fig. 6 for the CF_4-based gas mixture. In fact, this means that an increase in the O_2 content in the $C_4F_8/Ar/O_2$ gas mixture results in a weaker suppression of the polymerization through the bulk chemistry compared with the CF_4-based gas mixture. In addition, the low densities of the O and $O(^1D)$ atoms limit the formation rates for FO and CFO species in R33, R64, R67, and R69. Therefore, even in the presence of oxygen, the F atom formation rate is composed only of R11–R14 and has no support from both atom-molecular reactions and electron-impact dissociation of FO (R21) and CFO (R22). In such a situation, the F atom density decreases monotonically toward O_2-rich plasmas ($n_F = 8.0 \times 10^{12}$–8.6×10^{11} cm^{-3} for 0–50% O_2). Since R53 and R61 do not contribute to the formation rate of F_2 molecules, the F_2 density follows the density of the F atoms due to decreasing R64. A very weak change in the density of C_2F_4 (1.5×10^{13}–1.6×10^{13} cm^{-3} for 0–50% O_2) is because of the near-to-proportional decrease in their formation (R1, R3) and decay (R27) rates. The noticeable growth in n_{CF_4} (8.9×10^{12}–3.8×10^{13} cm^{-3} for 0–50% O_2) is due to an increase in their formation rate in R53, which is supported by increasing CFO density. In the CF_4-based plasma, this mechanism does not work because of the lower CF_3 radical density. It is worth mentioning that the behaviors of the CF, CF_2, and CF_2O species shown in Fig. 7 are in good agreement with the measured values reported by Xi Li et al. [19] In addition, the changes in O and F atom densities are quite close to those obtained experimentally by Takashi et al. [22]. This allows us to conclude that our model provides an adequate description of the main kinetic effects determining the composition of $C_4F_8/Ar/O_2$ plasma.

Finally, we would like to note that the decrease in the F atom density in the C_4F_8-based plasma does not directly mean a similar change in the etching rate, even if the etching process occurs in the reaction-rate-limited etching regime. Such a straightforward correlation will be valid only if the fluorocarbon polymer deposited on the surface does not inhibit the etching process. In reality, one can expect the etching rate to be influenced by at least two opposing factors. The first is a decrease in the F atom density and flux, as mentioned with reference to Fig. 7. The second is the acceleration of the polymer decomposition because of the increasing fluxes of O and $O(^1D)$. Obviously, the last effect causes an increase in the fraction of free surface suitable for the adsorption of F atoms and thus increases the probability of chemical reaction. Therefore, the dependence of the etching rate on the O_2 content in the feed gas easily forms a non-monotonic shape.

4. Conclusion

In this work, we compared $CF_4/O_2/Ar$ and $C_4F_8/O_2/Ar$ gas systems with the aim of understanding the influence of the substitution of Ar for O_2 at a fixed 50% fraction of the fluorocarbon gas on the plasma

parameters and densities of active species. It was found that, in both gas systems, an increase in the O_2 content in the feed gas in the range of 0–50% results in a similar change in the ion energy flux with an expected negative impact on the efficiency of the physical etching pathway. The main differences between the CF_4- and C_4F_8-based plasmas are in the chemistry of the neutral species. In the CF_4-based gas mixture, an increase in the O_2 component of the feed gas leads to a greater F atom density because of an effective realization of atom-molecular processes involving O and O(^{1}D) with the resulting electron-impact dissociation of fluorine-containing reaction products. In the C_4F_8-based plasma, the F atom density decreases monotonically toward more oxygenated gas mixtures. Here, the mechanisms discussed do not work because of the fast decay of O_2 in the reaction with CF and C species that predetermines the much lower densities of O and O(^{1}D).

Acknowledgments

This work was supported by the Industrial Strategic Technology Development Program (10041681, Development of Fundamental Technology for 10 nm process semiconductors and 10 G size large area processes with high plasma density and VHF condition) funded by the Ministry of Knowledge Economy (MKE, Republic of Korea).

References

[1] S.M. Rossnagel, J.J. Cuomo, W.D. Westwood, Handbook of Plasma Processing Technology, Noyes Publications, New Jersey, 1990.
[2] J.R. Rooth, Industrial Plasma Engineering, IOP Publishing LTD, Philadelphia, 1995.
[3] A.J. Roosmalen, J.A.G. Baggerman, S.J.H. Brader, Dry Etching for VLSI, Plenum Press, New York, 1991.
[4] S. Wolf, R.N. Tauber, Silicon Processing for the VLSI Era, Process Technology, vol. 1, Lattice Press, New York, 2000.
[5] T. Kimura, M. Noto, J. Appl. Phys. 100 (2006) 063303.
[6] I.C. Plumb, K.R. Ryan, Plasma Chem. Plasma Process. 6 (1986) 205.
[7] S.P. Venkatesan, I. Trachtenberg, T.F. Edgar, J. Electrochem. Soc. 137 (1990) 2280.
[8] P. Schoenborn, R. Patrick, H.P. Baltes, J. Electrochem. Soc. 136 (1989) 199.
[9] M. Kim, N.-K. Min, A. Efremov, H.W. Lee, C.-S. Park, K.-H. Kwon, J. Mater. Sci. Mater. Electron. 19 (2008) 957.
[10] T. Kimura, K. Hanaki, Jpn. J. Appl. Phys. 47 (2008) 8546.
[11] A.M. Efremov, D.-P. Kim, C.-I. Kim, Vacuum 75 (2004) 133.
[12] G. Kokkoris, A. Goodyear, M. Cooke, E. Gogolides, J. Phys. D. Appl. Phys. 41 (2008) 195211.
[13] A.V. Vasenkov, X. Li, G.S. Oehrlein, M.J. Kushner, J. Vac. Sci. Technol. A 22 (2004) 511.
[14] S. Rauf, P.L.G. Ventzek, J. Vac. Sci. Technol. A 20 (2002) 14.
[15] W.W. Stoffels, E. Stoffels, K. Tachibana, J. Vac. Sci. Technol. A 16 (1998) 87.
[16] T. Kimura, K. Ohe, J. Appl. Phys. 92 (2002) 1780.
[17] D. Bose, S. Rauf, D.B. Hash, T.R. Govindan, M. Meyyappan, J. Vac. Sci. Technol. A 22 (2004) 2290.
[18] K. Miyata, M. Hori, T. Goto, Jpn. J. Appl. Phys. 36 (1997) 5340.
[19] X. Li, L. Ling, X. Hua, M. Fukasawa, G.S. Oehrlein, M. Barela, H.M. Anderson, J. Vac. Sci. Technol. A 21 (2003) 284.
[20] K. Sasaki, Y. Kawai, K. Kadota, Rev. Sci. Instrum. 70 (1999) 76.
[21] K. Sasaki, Y. Kawai, C. Suzuki, K. Kadota, J. Appl. Phys. 83 (1998) 7482.
[22] K. Takashi, H. Katsuyuki, Jpn. J. Appl. Phys. 48 (2009) 096004.
[23] A. Efremov, N.-K. Min, B.-G. Choi, K.-H. Baek, K.-H. Kwon, J. Electrochem. Soc. 155 (2008) D777.
[24] A. Efremov, Y. Kim, H.-W. Lee, K.-H. Kwon, Plasma Chem. Plasma Process. 31 (2011) 259.
[25] E.O. Johnson, L. Malter, Phys. Rev. 80 (1950) 58.
[26] M. Sugavara, Plasma etching: Fundamentals and Applications, Oxford University Press, New York, 1998.
[27] T. Kimura, K. Ohe, Plasma Sources Sci. Technol. 8 (1999) 553.
[28] NIST Chemical Kinetics Database, http://kinetics.nist.gov/kinetics/index.jsp.
[29] M.A. Lieberman, A.J. Lichtenberg, Principles of Plasma Discharges and Materials Processing, John Wiley & Sons Inc., New York, 1994.
[30] C. Lee, D.B. Graves, M.A. Lieberman, Plasma Chem. Plasma Process. 16 (1996) 99.
[31] A.M. Efremov, D.P. Kim, C.I. Kim, IEEE Trans. Plasma Sci. 32 (2004) 1344.
[32] A.M. Efremov, D.P. Kim, C.I. Kim, Thin Solid Films 474 (2005) 267.
[33] B. Chapman, Glow Discharge Processes: Sputtering and Plasma Etching, John Wiley & Sons, New York, 1980.